IEEE Access
Multidisciplinary | Rapid Review | Open Access Journal

Received July 5, 2021, accepted August 11, 2021, date of publication August 18, 2021, date of current version August 27, 2021.

Digital Object Identifier 10.1109/ACCESS.2021.3105811

Reduced-Cost Microwave Design Closure by Multi-Resolution EM Simulations and Knowledge-Based Model Management

SLAWOMIR KOZIEL[1,2], (Senior Member, IEEE), ANNA PIETRENKO-DABROWSKA[2], (Senior Member, IEEE), AND PIOTR PLOTKA[2]

[1]Engineering Optimization and Modeling Center, Department of Technology, Reykjavik University, 102 Reykjavik, Iceland
[2]Faculty of Electronics, Telecommunications and Informatics, Gdańsk University of Technology, 80-233 Gdańsk, Poland

Corresponding author: Anna Pietrenko-Dabrowska (anna.dabrowska@pg.edu.pl)

This work was supported in part by the Icelandic Centre for Research (RANNIS) under Grant 217771, and in part by the National Science Centre of Poland under Grant 2020/37/B/ST7/01448.

ABSTRACT Parameter adjustment through numerical optimization has become a commonplace of contemporary microwave engineering. Although circuit theory methods are ubiquitous in the development of microwave components, the initial designs obtained with such tools have to be further tuned to improve the system performance. This is particularly pertinent to miniaturized structures, where the cross-coupling effects cannot be adequately accounted for using equivalent networks. For the sake of reliability, design closure is normally performed using full-wave electromagnetic (EM) simulation models, which entails considerable computational expenses, often impractically excessive. Available mitigation techniques include acceleration of the conventional (e.g., gradient-based) routines using adjoint sensitivities or sparse sensitivity updates, surrogate-assisted and machine learning algorithms, the latter often combined with nature-inspired procedures. Another alternative is the employment of variable-fidelity simulations (e.g., space mapping, co-kriging), which is most often limited to two levels of accuracy (coarse/fine). This work discusses an EM model management approach coupled with trust-region gradient-based routine, which exploits problem-specific knowledge for continuous (multi-level) modification of the discretization density of the microwave structure at hand in the course of the optimization run. The optimization process is launched at the lowest discretization level, thereby allowing for low-cost exploitation of the knowledge about the device under study. Subsequently, based on the convergence indicators, the model fidelity is gradually increased to ensure reliability. The simulation fidelity selection is governed by the algorithm convergence indicators. Computational speedup (i.e., reduction in the number of EM simulations required by the optimization process to converge) is achieved by maintaining low resolution in the initial stages of the optimization run, whereas design quality is secured by eventually switching to the high-fidelity model when close to concluding the process. Numerical verification is carried out using two microstrip circuits, a dual-band power divider and a dual-band branch-line coupler, with the average savings of almost sixty percent when compared to single-fidelity optimization.

INDEX TERMS Simulation-based optimization, microwave design, multi-fidelity simulations, model management, gradient-based search.

I. INTRODUCTION

The role of full-wave electromagnetic (EM) simulations has been gradually increasing in microwave design over the years [1]–[4]. Perhaps the major reason is that traditionally used analytical or network-equivalent tools are no longer adequate when EM cross-couplings [5], substrate anisotropy [6], the effects of environmental components (connectors, housing, nearby devices) [7], or multi-physics phenomena [8], are to be taken into account. At the same time, the

The associate editor coordinating the review of this manuscript and approving it for publication was Wenjie Feng.

topological complexity of microwave circuits has been gradually increasing to meet the stringent performance requirements pertinent to emerging areas (5G communications [9], energy harvesting [10], wireless power transfer [11], space applications [12]), to enable miniaturization [13]–[15], or to implement additional functionalities (dual-band [16], [17] or multi-band operation [18], [19], tunability [20], unconventional phase characteristics [21], etc.). Topologically sophisticated circuits are described by a large number of design variables that need to be simultaneously tuned in pursuit of controlling multiple performance figures and constraints. When conducted at the level of EM simulation models (otherwise mandatory to ensure reliability), the parameter adjustment process becomes a daunting task. The major challenge is high computational cost incurred by a typically large number of EM analyses associated with numerical optimization procedures. This cost may be impractical even for local search (both gradient-based [22], [23], and derivative-free [24] procedures), and it becomes prohibitive in the case of global optimization, especially when using population-based metaheuristics [25]–[28]. Similar issues arise while solving uncertainty quantification problems such as statistical analysis [29] or tolerance-aware design [30].

Given the aforementioned challenges, the development of more efficient optimization algorithms is a matter of practical necessity. A possible option is to accelerate evaluation of the system response gradients, which can be achieved using adjoint sensitivities [31], [32], mesh deformation methods [33], [34], or sparse Jacobian updates within gradient-based optimization procedures [35], [36]. Another possibility, which has been gaining an increasing popularity over the recent years, is the incorporation of surrogate modelling techniques [37], [38]. Two major classes thereof can be distinguished, data-driven [39], and physics-based ones [40]. The models of the former group are more popular, cheap to evaluate, generic, and easily accessible (e.g., [41], [42]). Some of widely used methods include kriging [43], radial basis functions [44], neural networks [45], support vector regression [46], and polynomial chaos expansion [47]. Unfortunately, a construction of accurate surrogates of microwave components is severely hindered by the curse of dimensionality. A popular approach is to combine a number of approximation models are often combined with sequential design of experiments techniques [48] to enable accelerated globalized search [49], also in conjunction with nature-inspired algorithms [50]–[52]. Still, practical applicability of such methods is in most cases limited to structures described by few parameters [53], [54]. Physics-based surrogates are more immune to dimensionality issues due to being based on the problem-specific knowledge embedded in the underlying low-fidelity models (e.g., equivalent networks) [55]. For the same reason, these methods are less versatile. Popular techniques of this group include space mapping [56], response correction methods [57], [58], cognition-driven design [59], or feature-based optimization [60].

Although the relevance of global search is undeniable in certain application areas such as antenna array pattern synthesis [61], design of frequency selective surfaces [62], or metasurfaces for stealth technology [63], as well as parameter tuning of CMRC-based compact microstrip components [64], majority of typical EM-driven scenarios involve local optimization. In many cases, reasonable starting points can be identified using circuit-theory tools, so that dramatic alterations of geometry parameters are often unnecessary. As outlined above, expediting local procedures (in particular, gradient-based algorithms) can be achieved using adjoint sensitivities, yet it is an intrusive technique, which is not widespread in commercial simulation packages. Whereas purely algorithmic means such as sparse sensitivity updates (e.g., involving design relocation [65] or Jacobian change tracking [66], Broyden-based schemes [67]), may result in over fifty percent speedup with a certain degradation of design quality. Variable-fidelity methods such as space mapping [56] can be extremely efficient, yet their performance is highly dependent on the optimization framework setup (low-fidelity model selection [68], model correction technique [69]). The employment of multi-fidelity simulation models may lead to additional benefits. In particular, sequential application of two or more resolutions potentially allows for further acceleration [70]. However, a practical issue remains model management: selecting the right discretization levels as well as the criteria for switching between the models is not a trivial endeavour; both factors affect the reliability and computational complexity of the optimization process [71].

In this work, a novel optimization procedure is proposed, which incorporates multi-resolution EM simulation models into the gradient-based algorithm. The discretization level of the structure under design is selected from the predefined spectrum of resolutions allocated between the lowest usable fidelity, and the high-fidelity representation (established to render the ultimate level of accuracy according to the designer's needs). Appropriate assessment of the admissible spectrum of model fidelities requires exploiting problem-specific knowledge and allows for achieving a significant acceleration of optimization process without considerable deterioration of the design quality. The model fidelity utilized at any particular stage of the optimization process is correlated to convergence status of the algorithm, with the model resolution gradually increased towards the end of the procedure to ensure reliability. Here, in order to extract the information about the optimization process status and performance, convergence indicators have been defined that are utilized for governing model fidelity adjustment throughout the entire process. Numerical verification of the algorithm is carried out using two microstrip circuits, a dual-band branch-line coupler and a dual-band power divider. In both cases, the computational efficiency of the proposed technique by far exceeds that of the conventional (high-fidelity model only) optimization with the average savings of almost sixty percent. At the same time, degradation of

the design quality is negligible. To the best knowledge of the authors, the presented approach is the first attempt to develop a rigorous model management strategy capable of handling a continuous spectrum of computational model fidelities. The framework can be considered a step towards improving the efficacy of EM-driven design optimization procedures by the employment of multi-resolution simulations.

II. MULTI-RESOLUTION MODELS AND KNOWLEDGE-BASED MODEL MANAGEMENT FOR EXPEDITED OPTIMIZATION OF MICROWAVE COMPONENTS

The purpose of this section is to introduce a methodology incorporating multi-resolution EM simulations into the gradient-based optimization procedure. The fundamental component of the presented approach is a knowledge-based strategy for handling variable-fidelity models in the course of the optimization run. In order to expedite the parameter adjustment process, coarse-discretization simulations are employed in the early stages, gradually replaced by finer-discretization ones when approaching convergence, which is to ensure reliability. The developed model management scheme is generic in the sense that it can be embedded into any iterative search procedure of a descent type. Notwithstanding, for the sake of demonstration, in this work, it is combined with the trust-region algorithm. The remaining part of this section is organized as follows. Section II.*A* formulates the design closure task, whereas Section II.*B* recalls the standard trust-region gradient-based optimization algorithm. Multi-resolution models are discussed in Section II.*C*. Sections II.*D* and II.*E* outline the model management scheme and the entire optimization procedure, respectively.

A. MICROWAVE DESIGN CLOSURE

The final adjustment of geometry parameters (also referred to as design closure) is necessary to account for inaccuracies of the prior design stages, often performed using circuit theory tools [72]. At times, especially in the case of miniaturized structures implemented using, e.g., compact microstrip resonant cells (CMRCs), the parameter tuning needs to be more invasive because even identification of a reasonable initial design might be challenging. Numerically rigorous design closure requires a definition of the quality metric, which, in practice, needs to accommodate two or more objectives, such as the operating bandwidth, power split ratio, port isolation, or the phase relationships between the input and output signals. This works addresses single-objective optimization (as opposed to genuine multi-objective design, e.g., [27], [52]). Handling of several figures of merit is tackled by the assignment of a primary objective and controlling the remaining ones through appropriately defined constraints.

To formulate the design closure task, we will denote as $\boldsymbol{x} = [x_1 \ldots x_n]^T$ the vector of independent parameters of the microwave component of interest. We aim at solving

$$\boldsymbol{x}^* = \arg\min_{\boldsymbol{x}} U(\boldsymbol{x}) \tag{1}$$

subject to inequality constraints $g_k(\boldsymbol{x}) \leq 0$, $k = 1, \ldots, n_g$, and equality constraints $h_k(\boldsymbol{x}) = 0$, $k = 1, \ldots, n_h$. Because the constraints are often related to the electrical characteristics of the structure, they are expensive to evaluate (EM simulation is required). Consequently, their explicit treatment is inconvenient. In this work, implicit handling using a penalty function approach is used [73]. In particular, the parameter adjustment problem is reformulated as follows:

$$\boldsymbol{x}^* = \arg\min_{\boldsymbol{x}} U_P(\boldsymbol{x}) \tag{2}$$

where the function U_P takes the form of

$$U_P(\boldsymbol{x}) = U(\boldsymbol{x}) + \sum\nolimits_{k=1}^{n_g+n_h} \beta_k c_k(\boldsymbol{x}) \tag{3}$$

The penalty functions $c_k(\boldsymbol{x})$ are introduced to measure violations of the constraints (here, inequality and equality constraints are handled together), whereas β_k stand for the penalty coefficients. The values of β_k are normally selected to ensure that the contributions of the penalty terms are noticeable as compared to the primary objective if violations of the respective constraints are beyond acceptable levels.

Let us consider some examples. In the following, the circuit scattering parameters will be denoted as $S_{kl}(\boldsymbol{x}, f)$, where f stands for the frequency, and $\boldsymbol{x}$, as before, represents the vector of designable variables; k and l are denote the circuit ports.

- Design of a dual-band coupler assuming the operating frequencies f_1 and f_2. The requirements are: (i) ensuring equal power split at both f_1 and f_2, (ii) minimization of the circuit matching and isolation responses (also at both operating frequencies). In this case, the second requirement is selected as a primary objective and treated in a minimax sense because the achievable levels of neither matching nor isolation responses are not known beforehand. The first requirement is handled through an equality constraint. Consequently, the objective function U_P takes the form of

$$\begin{aligned} U_P(\boldsymbol{x}) = {} & \max\{S_{11}(\boldsymbol{x}, f_1), S_{11}(\boldsymbol{x}, f_2), \\ & S_{41}(\boldsymbol{x}, f_1), S_{41}(\boldsymbol{x}, f_2)\} \\ & + \beta[|S_{21}(\boldsymbol{x}, f_1) - S_{31}(\boldsymbol{x}, f_1)|^2 \\ & + |S_{21}(\boldsymbol{x}, f_2) - S_{31}(\boldsymbol{x}, f_2)|^2] \end{aligned} \tag{4}$$

- Design of a triple-band power divider assuming the operating frequencies f_1, f_2, and f_3. The requirements are: (i) ensuring equal power split at all operating frequencies, (ii) minimization of the circuit input matching $|S_{11}|$, output matching $|S_{22}|$ and $|S_{33}|$, (iii) minimization of isolation $|S_{23}|$ (both (ii) and (iii) at f_1, f_2, and f_3). Similarly as in the previous example, the equal power

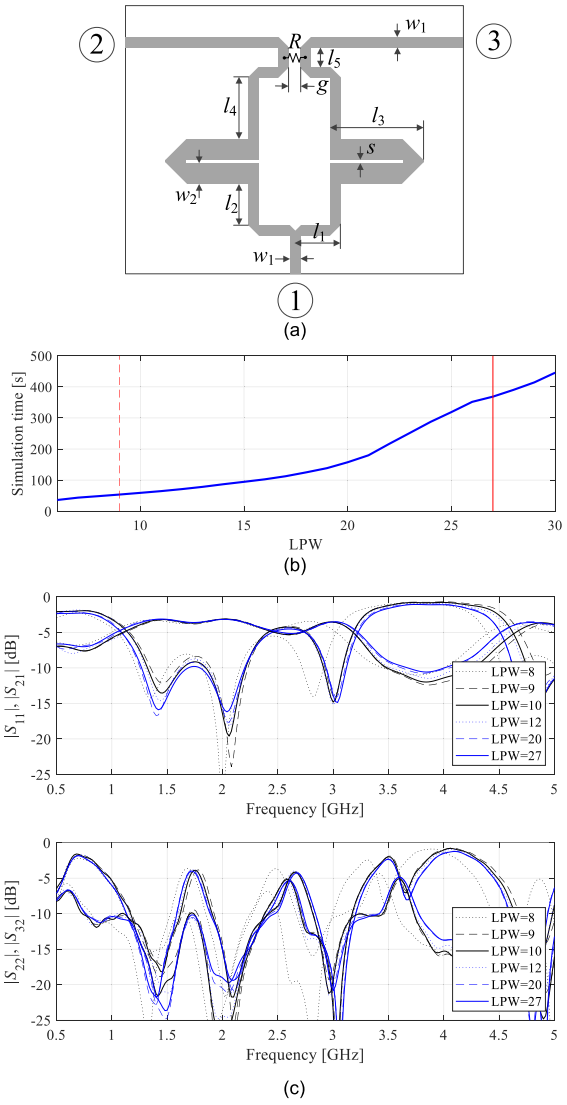

FIGURE 1. Multi-resolution EM-simulation models for a dual-band power divider: (a) circuit geometry, (b) simulation time versus discretization density of the structure (governed by the lines-per-wavelength parameter, LPW), (c) selected *S*-parameter characteristics corresponding to the selected values of LPW. The discretization densities corresponding to the high-fidelity model (- - -), and the lowest usable low-fidelity one (–), are marked using the vertical lines.

split requirement will be treated as constraint, whereas the remaining specifications will be minimized in a minimax sense. The objective function takes the form of

$$U_P(\boldsymbol{x}) = \max\left\{\max_{k,l\in\{1,2,3\}} S_{kk}(\boldsymbol{x},f_l),\ \max_{l\in\{1,2,3\}} S_{23}(\boldsymbol{x},f_l)\right\} + \beta\sum_{l=1}^{3}|S_{21}(\boldsymbol{x},f_l)-S_{31}(\boldsymbol{x},f_l)|^2 \tag{5}$$

If the geometrical symmetry of the circuit ensures satisfaction of the equal power split condition, the second term in (5) becomes redundant.

B. TRUST-REGION GRADIENT-BASED OPTIMIZATION ALGORITHM

As mentioned at the beginning of this section, the proposed approach to multi-resolution optimization can be incorporated into various iterative search procedures. Here, for the sake of illustration, it is combined with the trust-region (TR) gradient-based algorithm [74], which is briefly recalled in the remaining part of this sub-section. In Section III, the TR procedure utilizing the high-fidelity model is also used as a reference method to determine the computational benefits of the methodology proposed in this paper.

The idea behind the TR procedure is to approximate the solution $\boldsymbol{x}^*$ to (2) with a series of parameter vectors $\boldsymbol{x}^{(i)}$ produced by solving the sub-problems

$$\boldsymbol{x}^{(i+1)} = \arg\min_{||\boldsymbol{x}-\boldsymbol{x}^{(i)}||\le d^{(i)}} U_L^{(i)}(\boldsymbol{x}) \tag{6}$$

in which the objective function $U_L^{(i)}$ is of the same form as the function U_P except that it is defined at the level of the local approximation model of the system characteristics rather than directly the EM-simulated outputs. Here, a linear expansion model is used, which, for the scattering parameter S_{kl}, takes the form of

$$S_{kl.L}^{(i)}(\boldsymbol{x},f) = S_{kl}(\boldsymbol{x}^{(i)},f) + \boldsymbol{G}_{kl}(\boldsymbol{x}^{(i)},f)\cdot(\boldsymbol{x}-\boldsymbol{x}^{(i)}) \tag{7}$$

Similarly as in (7), $\boldsymbol{x}^{(i)}$ is the current iteration point, whereas $\boldsymbol{G}_{kl}\ (x^{(i)},f)$ stands for the gradient of S_{kl} at $\boldsymbol{x}^{(i)}$ and frequency f. The gradients are obtained through finite differentiation at the cost of n additional EM simulations of the circuit under optimization (recall that n is the number of independent parameters). The trust region size $d^{(i)}$ is updated after each iteration; in particular, it is increased if the gain ratio $r = [U_P(\boldsymbol{x}^{(i)+1}) - U_P(\boldsymbol{x}^{(i)})]/[U_L^{(i)}(\boldsymbol{x}^{(i+1)}) - U_L^{(i)}(\boldsymbol{x}^{(i)})$ is sufficiently large (e.g., > 0.75), and decreased if r is too small (e.g., < 0.25). Also, the new point $\boldsymbol{x}^{(i+1)}$ is only accepted if the improvement of the primary objective function has been observed, i.e., $U_P(\boldsymbol{x}^{(i+1)}) < U_P(\boldsymbol{x}^{(i)})$. If this is not the case, the iteration is repeated with a reduced d (as $r < 0$). As highlighted in the introduction, the procedure (6), (7) can be expedited by the incorporation adjoint sensitivities [31], [32], or sparse sensitivity updates [35], [67]. These will not be addressed in this work further because either can be combined with the presented multi-resolution scheme as independent acceleration mechanisms.

C. MULTI-RESOLUTION EM SIMULATIONS

Multi-resolution or multi-fidelity EM simulations are utilized in this work to improve the computational efficiency of the microwave design optimization process. The introductory section indicated that variable-fidelity techniques have becoming increasingly popular over the recent years. Yet, the majority of available techniques employ two models, often referred to as low-fidelity (or coarse) and high-fidelity (or fine). Furthermore, the low-fidelity model is often a simplified-physics representation (e.g., equivalent network in the case of microwave circuits [55]). A typical way of

incorporating low-fidelity data is through appropriate correction (e.g., space mapping [40], adaptive response correction [75], manifold mapping [76]). Another approach is to enable reduced-cost parameter space exploration within machine learning frameworks [49], or to exploit model correlations in variable-fidelity modelling methods such as co-kriging [77]. Perhaps the most serious inconvenience associated with these methods is a need to properly set up (or construct for that matter) the low-fidelity model. Both the quality and the computational cost of the latter (in relation to the high-fidelity model) affect the efficacy of the optimization process [71].

Consider a family of scattering parameter characteristics of a dual-band power divider (see Section III.*A* for a description of the circuit geometry) shown in Fig. 1(c). The responses are obtained through full-wave EM simulation at different levels of resolution, parameterized by means of the lines-per-wavelength (LPW) coefficient, using the time-domain solver of CST Microwave Studio. Figure 1(b) shows the simulation time versus LPW. The plots illustrate typical relationships between the model resolution, evaluation time, and the simulation reliability. In particular, reducing the discretization density beyond a certain level (here, LPW = 9), makes the model unusable because it no longer represents the circuit behaviour in an adequate manner. On the other hand, increasing discretization density leads to a saturation, where the EM-simulated responses essentially converge. Here, LPW = 27 can be considered as corresponding to the high-fidelity representation of the structure. In the following, that lowest usable LPW will be denoted as $L_{\min}$, whereas the LPW corresponding to the high-fidelity model will be denoted as $L_{\max}$.

The purpose of this paper is to employ the simulation models within the resolution range $L_{\min} \leq L \leq L_{\max}$, in pursuit of achieving computational savings while retaining the reliability. The former will be ensured by using low-fidelity models in the early stages of the optimization process, whereas the latter is secured by switching towards high-fidelity simulations when close to the conclusion of the optimization run. The main assumptions behind the developed model management strategy, as well as model resolution adjustment scheme, will be described in Section II.*D*.

D. OPTIMIZATION PROCEDURE

We aim at adjusting the fidelity of the EM simulation in the course of the optimization algorithm run so as to reduce the computational cost of the process while retaining the reliability. The optimization routine is assumed to work iteratively by generating subsequent approximations $\boldsymbol{x}^{(i)}$ to the optimum design $\boldsymbol{x}^*$. As mentioned before, in this work, the method of choice is the trust-region gradient-based algorithm recalled in Section II.*B*. The model resolution is controlled by means of the parameter L (the lines-per-wavelength, LPW, in the case of CST Microwave Studio), ranging from $L_{\min}$ (lowest usable discretization density) to $L_{\max}$ (high-fidelity model). The model management scheme should comply with the following recommendations:

- The lowest-resolution computational model should be employed at the beginning of the optimization run. This is to ensure a reduction of the CPU cost of the optimization process because the largest design relocations are normally undertaken at the early stages, i.e., away from the optimum design;
- The highest-resolution model should be used towards the end of the optimization run so as the reliability of the process is ensured;
- The convergence status of the algorithm should be used to control the adjustment of the model resolution because the indicators such as $||\boldsymbol{x}^{(i+1)} - \boldsymbol{x}^{(i)}||$, the trust-region radius $d^{(i)}$, or the objective function improvement $U_P(\boldsymbol{x}^{(i)}+1)) - U_P(\boldsymbol{x}^{(i)})$ are the most straightforward metrics to determine the current stage of the optimization process;
- The adjustments of the model resolution should be carried out in a smooth manner (i.e., without discontinuities, or large 'jumps'), so that the stability of the optimization process is facilitated.

In order to formulate the model management scheme, we also need to specify the termination criteria of the optimization algorithm, and the associated termination thresholds. The termination condition will be defined as follows:

$$\begin{aligned} &||\boldsymbol{x}^{(i+1)} - \boldsymbol{x}^{i}|| < \varepsilon_x \quad \text{OR } d^{(i)} < \varepsilon_x \\ &\text{OR } \ |U_P(\boldsymbol{x}^{(i+1)}) - U_P(\boldsymbol{x}^{(i)})| < \varepsilon_U \end{aligned} \tag{8}$$

where ε_x and ε_U are the user-defined thresholds. The particular values employed in the numerical experiments of Section III are $\varepsilon_x = 10^{-3}$, and $\varepsilon_U = 10^{-3}$.

As we need to gather information about the optimization course, the convergence status of the algorithm at the ith iteration will be quantified using the parameter $F^{(i)}$, defined as

$$F^{(i)}(\varepsilon_x, \varepsilon_U) = \max\left\{\frac{\varepsilon_x}{||\boldsymbol{x}^{(i+1)} - \boldsymbol{x}^{(i)}||}, \frac{\varepsilon_U}{|U_P(\boldsymbol{x}^{(i+1)}) - U_P(\boldsymbol{x}^{(i)})|}\right\} \tag{9}$$

The adjustment of the model resolution, i.e., the determination of the fidelity parameter $L^{(i)}$ at the ith iteration of the optimization routine will be realized according to the following formula

$$L^{(i+1)} = \begin{cases} L_{\min} \text{ if } F^{(i)}(\varepsilon_x, \varepsilon_U) \leq M \\ \max\left\{L^{(i)}, L_{\min} + (L_{\max} - L_{\min})\left[F^{(i)}(\varepsilon_x, \varepsilon_U) - M\right]^{\frac{1}{\alpha}}\right\} \end{cases} \tag{10}$$

In (10), there are two control parameters, M and α. The former determines the algorithm convergence level at which the model resolution is supposed to start increasing. In our numerical experiments we use $M = 10^{-2}$ meaning that the current design relocation (or objective function changes) exceeds by about two orders of magnitude the termination

thresholds. This value is reasonable to ensure that a sufficient number of initial iterations are executed using the lowest-fidelity model, leading to considerable computational savings. The second coefficient is a shape parameter that decides upon how fast the discretization level is altered as a function of $F^{(i)}$.

The above scheme has to be enhanced to ensure that the high-fidelity model will be used at a certain stage of the optimization process. This is not guaranteed by (10) because—whenever one or more iterations of the TR algorithm are rejected due to the lack of improvement of the objective function (i.e., when $U_P(\boldsymbol{x}^{(i+1)}) \geq U_P(\boldsymbol{x}^{(i)})$—the process will be terminated by shrinking the TR radius $d^{(i)}$ with the model resolution set to the current LPW (not necessarily $L_{\max}$). The involvement of the high-fidelity model is secured by introducing a supplementary mechanism, launched upon the algorithm termination. More specifically, the following action is executed

$$\text{IF } L^{(i)} < L_{\max} \text{ THEN } L^{(i+1)} = L_{\max} \text{ AND } d^{(i+1)} = M_d \varepsilon_x \tag{11}$$

If the EM model used upon termination was of lower fidelity than $L_{\max}$, the condition (11) enforces execution of further iterations with L set to $L_{\max}$. The multiplication factor M_d (set to 11 in the verification experiments of Section III) is to make sufficient room for design improvement during these additional iterations. Otherwise, the algorithm would converge immediately as the termination condition still holds with unaltered $\boldsymbol{d}^{(i)}$.

In order to expedite the optimization process further, the estimation of the system sensitivities (normally carried out by means of finite differentiation, cf. Section II.*B*) can be executed using the lower-fidelity model than the one employed for response evaluation. In particular, given the current discretization level $L^{(i)}$, the sensitivities are evaluated at the fidelity level L_{FD} determined as

$$L_{FD} = \max\left\{L_{\min}, \lambda L^{(i)}\right\} \tag{12}$$

Here, $0 \leq \lambda \leq 1$ is a control parameter of the algorithm, which, in the verification experiments will be set to $\lambda = 2/3$. The above mechanism capitalizes on the fact that although models of different resolutions may be misaligned, they share a common physical background, and are likely to exhibit a high level of correlation (which implies good alignment at the level of response derivatives). Furthermore, the correlations will improve with the increasing values of $L^{(i)}$, i.e., possible errors of rendering the Jacobian matrix due to (12) will diminish when close to convergence.

E. PROPOSED OPTIMIZATION ALGORITHM

The purpose of this section is to put together the algorithmic components described in Sections II.*A* through II.*D*. For the convenience of the reader, the control parameters of the procedure are recalled in Table 1.

1. Set the iteration index $i = 0$;
2. Set $L^{(i)} = L_{\min}$;
3. Evaluate circuit response $\boldsymbol{S}(\boldsymbol{x}^{(i)})$ at the resolution level $L^{(i)}$;
4. Evaluate circuit sensitivities $\boldsymbol{J}_S(\boldsymbol{x}^{(i)})$ at the resolution level L_{FD} (cf. (11));
5. Construct a linear model $\boldsymbol{L}^{(i)}(\boldsymbol{x}) = \boldsymbol{S}(\boldsymbol{x}^{(i)}) + \boldsymbol{J}_S(\boldsymbol{x}^{(i)}) \cdot (\boldsymbol{x} - \boldsymbol{x}^{(i)})$;
6. Obtain the design $\boldsymbol{x}^{(i+1)}$ by solving (6);
7. Evaluate circuit response $\boldsymbol{S}(\boldsymbol{x}^{(i+1)})$ at the resolution level $L^{(i)}$;
8. Update trust-region radius $d^{(i)}$ [74];
9. **if** $U_P(\boldsymbol{x}^{(i+1)}) < U_P(\boldsymbol{x}^{(i)})$
   Compute $L^{(i+1)}$ using(10);
   Set $i = i + 1$;
   end
10. **if** $||\boldsymbol{x}^{(i+1)} - \boldsymbol{x}^{(i)}|| < \varepsilon_x$ OR $d^{(i)} < \varepsilon_x$ OR $|U_P(\boldsymbol{x}^{(i+1)}) - U_P(\boldsymbol{x}^{(i)})| < \varepsilon_U$
    if $L^{(i)} < L_{\max}$
     Set $L^{(i)} = L_{\max}$ and modify $d^{(i)}$ according to (10); go to 3;
    else
     Go to 11;
    end
   else
    Go to 3;
   end
11. END.

FIGURE 2. Pseudocode of the proposed multi-resolution optimization procedure. All relevant EM-simulated responses of the circuit of interest are aggregated into $\boldsymbol{S(x)}$, whereas $\boldsymbol{J_S(x)}$ denotes the Jacobian matrix at the design $\boldsymbol{x}$.

TABLE 1. Control parameters of the multi-fidelity optimization procedure.

Parameter	Parameter role	Default value
ε_x, ε_U	Algorithm termination thresholds (Section II.*D*)	10^{-3}
M	Factor governing the initialization of the discretization level increase (Section II.*D*)	10^{-2}
α	Shape parameter for model resolution adjustment (Section II.*D*)	3
λ	Control parameter for setting discretization level L_{FD} for finite differentiation (Jacobian matrix computation) according to (11)	2/3
M_d	Multiplication factor for increasing TR radius in (10)	10

Among the parameters listed in Table 1, the termination thresholds are determined by the user to adjust the resolution of the optimization process. In the case of microstrip structures, 10^{-3} is normally more than sufficient given that most of the geometry parameters are in millimeters. The default values for other parameters, shown in the last column of Table 1 have been discussed before.

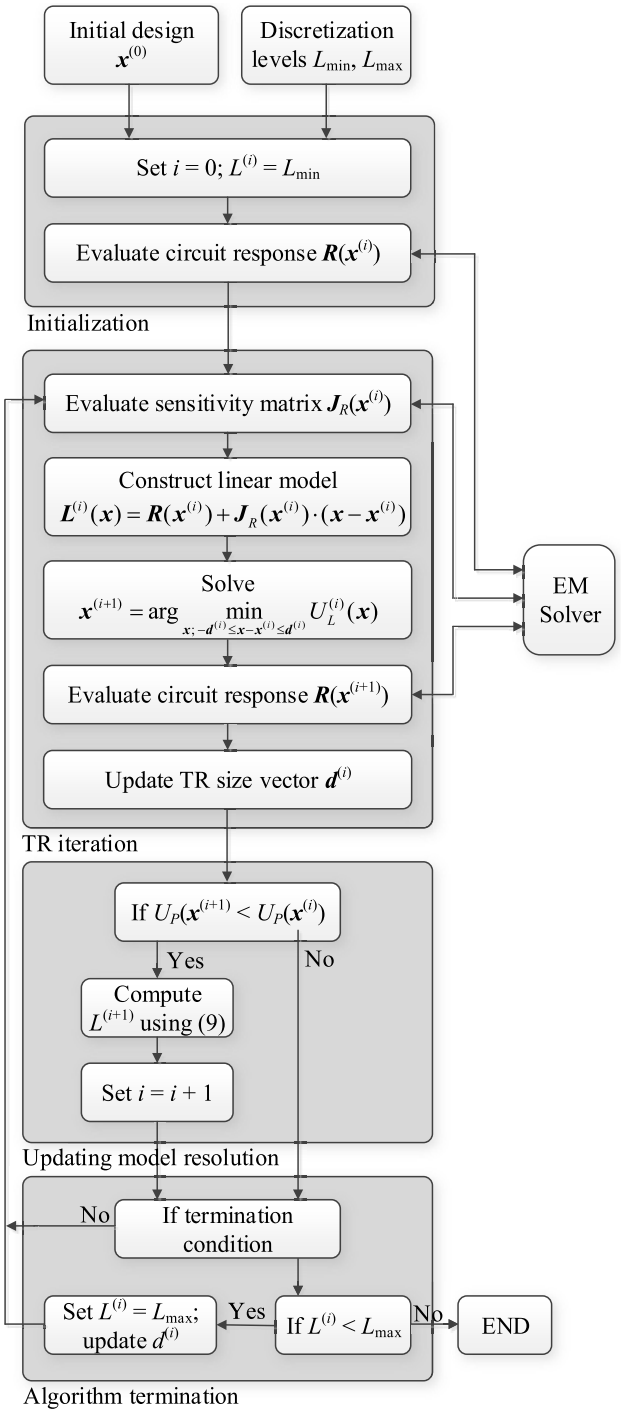

FIGURE 3. Flow diagram of the proposed multi-resolution optimization procedure.

The minimum and the maximum resolution levels L_{min} and L_{max} (see Section II.*C* for more details) are structure dependent and are normally determined based on initial simulations of the circuit and a visual inspection of the frequency characteristics. In particular, L_{max} (high-fidelity model) is the level that ensures sufficient simulation accuracy (according to the user needs), whereas L_{min} is the lowest resolution that still ensures adequate representation of the relevant response features (cf. Fig. 1).

Figure 2 shows the pseudocode of the algorithm. Therein, the EM-evaluated system responses are aggregated as $\boldsymbol{S}(\boldsymbol{x})$; the symbol $\boldsymbol{J}_S(\boldsymbol{x})$ stands for the Jacobian matrix, both at the design $\boldsymbol{x}$. The initial design is denoted as $\boldsymbol{x}^{(0)}$. For the sake of supplementary clarification, Figure 3 shows the flow diagram of the multi-fidelity optimization procedure.

III. NUMERICAL RESULTS

This section describes the verification cases studies undertaken to investigate the properties of the multi-resolution procedure discussed in Section II. The results obtained for two microstrip circuits, an equal split dual-band power divider, and a dual-band branch-line coupler are compared to the conventional, single-fidelity approach exclusively based on high-fidelity computational model of the respective structures. The points of interest include the computational speedup obtained using the multi-resolution model management, but also the optimization process reliability as compared to the reference.

A. CASE 1: DUAL-BAND POWER DIVIDER

The first verification example is a dual-band equal split power divider [78]. The circuit geometry is shown in Fig. 4. The structure is implemented on AD250 substrate ($\varepsilon_r = 2.5$, $h = 0.81$) mm, tan ($\delta = 0.0018$). The independent design variables are $\boldsymbol{x} = [l_1\ l_2\ l_3\ l_4\ l_5\ s\ w_2]^T$ (dimensions in mm); $w_1 = 2.2$ is fixed to ensure 50-ohm line impedance; $g = 1$ mm. The divider is simulated using the time-domain solver of CST Microwave Studio (~200,000 mesh cells, simulation time ~2 minutes). All the simulations were performed on Intel Xeon 2.1 GHz dual-core CPU, 128 GB RAM.

The goal is to optimize the geometry parameters with respect to the following objectives:

- The circuit operates at the frequencies $f_1 = 2.4$ GHz and $f_2 = 3.8$ GHz;
- Input matching $|S_{11}|$ and output matching $|S_{22}|$, $|S_{33}|$, are minimized within the frequency bands $[f_1 - 100$ MHz, $f_1 + 100$ MHz] and $[f_2 - 100$ MHz, $f_2 + 100$ MHz];
- Port isolation $|S_{23}|$ is minimized within the frequency bands $[f_1 - 100$ MHz, $f_1 + 100$ MHz] and $[f_2 - 100$ MHz, $f_2 + 100$ MHz];
- Equal power split is ensured.

The objective function for the optimization task is based on (5); however, the penalty term is not implemented because the equal power split condition is implied by the structure symmetry.

The lowest and the highest resolution levels for this structure were set to $L_{min} = 9$, and $L_{max} = 27$, respectively. The corresponding simulation times are 52 and 360 seconds, respectively. The relationship between the model resolution and the evaluation time has been shown in Fig. 1(b). Note that the time evaluation ratio between the high- and the lowest-fidelity models is almost seven, which allows us to anticipate that the computational speedup obtainable through multi-resolution approach may be considerable.

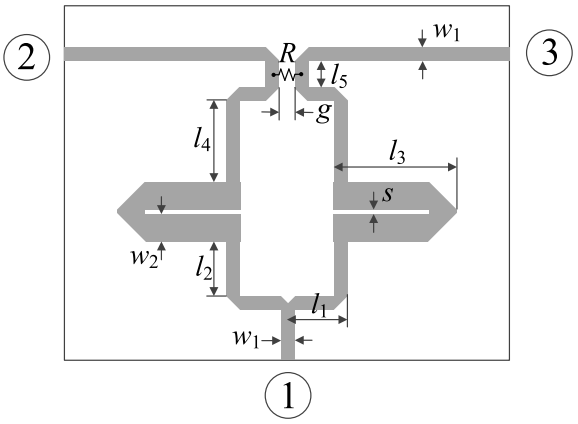

FIGURE 4. Dual-band equal split power divider [78]: circuit topology; ports marked using numbers in circles. Lumped resistor denoted as *R*.

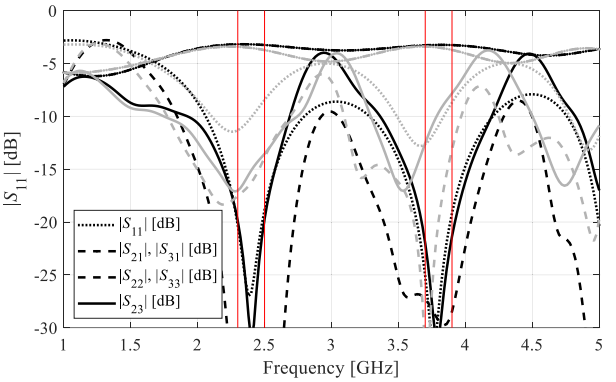

FIGURE 5. Frequency responses of the power divider of Fig. 4 for the representative run of the proposed multi-resolution algorithm. Target operating bandwidths marked using the vertical lines. The responses at the initial and the final design marked using gray and black colors, respectively.

As the optimization algorithm under consideration is a local search procedure, verification and benchmarking has been conducted based on ten independent runs initiated from different starting points. This is to reduce a possible bias caused by the dependence of the optimization outcome on the initial conditions. The benchmark is the standard TR algorithm of Section 2.2. There are three criteria considered when evaluating the algorithm performance:

- Computational cost, which for the multi-resolution algorithm is expressed in the equivalent number of high-fidelity model evaluations (i.e., by taking into account the time evaluation ratios between the high-fidelity and the current models utilized during particular iterations of the optimization algorithm);
- Quality of the design, measured using the objective function value averaged over all optimization runs executed for the considered problem;
- Reliability, understood as repeatability of results, quantified by means of the standard deviation of the objective function value (or the values of the relevant performance figures) over all optimization runs.

As the optimization process is never perfect due to the presence of numerical noise or possible multimodality, the standard deviation is expected to be strictly larger than zero even for the reference algorithm. Consequently, when evaluating reliability of the multi-resolution algorithm, its corresponding standard deviation should be compared to that of the reference algorithm rather than to the zero value. The values of the control parameters for the multi-resolution algorithm are the same as those listed in Table 1.

The numerical results have been gathered in Table 2. Furthermore, the initial and optimized divider characteristics obtained for the selected run of the multi-resolution procedure have been shown in Fig. 5. It can be observed that the proposed approach enables considerable computational savings which are close to seventy percent when compared to the reference algorithm. In other words, the optimization process is three times faster when using variable-fidelity model versus high-fidelity model only version. At the same time, no quality degradation has been observed: the average objective function values are identical for both methods. In terms of result repeatability, the proposed approach exhibits a certain advantage but the differences are statistically insignificant.

TABLE 2. Numerical results for power divider of Fig. 4.

Algorithm	Performance figure				
	Cost[1]	Cost savings[2]	U_P[3] [dB]	ΔU_P[4] [dB]	StdU_P[5] [dB]
Conventional TR search	91.9	-	–17.2	-	1.8
Multi-resolution (this work)	31.7	66%	–17.2	–0.2	1.6

[1] Number of equivalent high-fidelity EM simulations (averaged over ten algorithm runs).
[2] Relative computational savings in percent w.r.t. the reference algorithm.
[3] Objective function value (cf. (5)), averaged over ten algorithm runs.
[4] Degradation of the objective function value w.r.t. the reference algorithm, averaged over ten algorithm runs.
5 Standard deviation of the objective function value over the performed algorithm runs.

B. CASE II: DUAL-BAND BRANCH-LINE COUPLER

The second verification case is a dual-band branch line coupler (BLC) [17] implemented on the RO4003 substrate ($\varepsilon_r = 3.5$, $h = 0.51$) mm, tan ($\delta = 0.0027$). The circuit geometry has been shown in Fig. 6. There are nine independent design variables $\boldsymbol{x} = [L_s\ W_s\ l_{3r}\ w_1\ w_2\ w_3\ w_4\ w_5\ w_v^T]$ (dimensions in mm, except l_{3r}, which is unitless). We also have the following relationships: $d_L = d_W = 10$ mm, $L = 2\,d_L + L_s$, $W = 2\,d_W + 2\,w_1 + (W_s - 2\,w_f)$, $l_1 = W_s/2$, $l_2 = l_3 2^{1/2}$, $l_3 = l_{3r}((L_s - w_3)/2 - w_4/2^{1/2})$, $l_v1 = l_3/3$, and $l_v3 = L_s/2 - w_3/2 - l_3 + lv1$; the input/output line width w_f is fixed to 1.15 mm to ensure 50-ohm impedance. The EM simulation model is implemented in CST Microwave Studio, and evaluated using the time domain solver (∼150,000 mesh cells, simulation time about two minutes). The simulations were

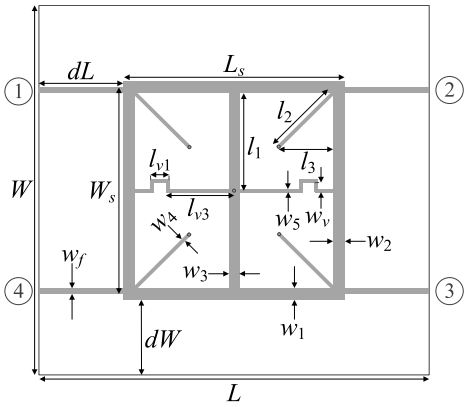

FIGURE 6. Dual-band branch-line coupler [17]: circuit topology; ports marked with numbers in circles.

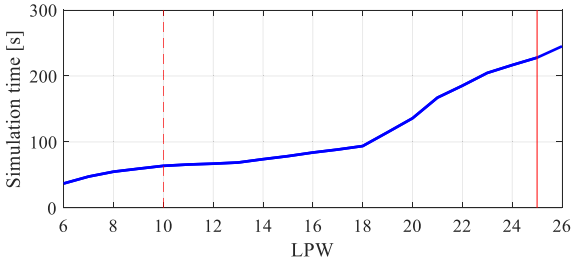

FIGURE 7. Dual-band branch-line coupler of Fig. 6: simulation time versus EM simulation fidelity. Vertical lines denote the resolution levels corresponding to L_{min} (- - -) and L_{max} (–).

performed on Intel Xeon 2.1 GHz dual-core CPU, 128 GB RAM.

The BLC in Fig. 6 is supposed to operate at the frequencies $f_1 = 1.8$ GHz and $f_2 = 3.4$ GHz. The design objective are as follows:

- Minimize the input matching $|S_{11}|$ and isolation $|S_{41}|$ at both f_1 and f_2;
- Ensure equal power split, i.e., $|S_{21}| = |S_{31}|$ at f_1 and f_2.

The objective function for this problem takes the form of (4), one of the examples considered in Section 2.1.

The lowest and the highest resolution levels for this structure were set to $L_{min} = 10$, and $L_{max} = 25$, respectively. The corresponding simulation times are 64 and 230 seconds, respectively. The relationship between the model resolution and the evaluation time has been shown in Fig. 7. For this circuit, the time evaluation ratio between the high- and the lowest-fidelity models is less than four, therefore, the expected computational savings are not as significant as for the first verification case.

The arrangement of the numerical experiments is the same as described in Section 3.1, i.e., ten independent algorithms runs (both the multi-resolution method and the reference algorithm) using different starting points. The values of the control parameters for the multi-resolution algorithm are the same as those listed in Table 1.

Table 3 provides the numerical results, whereas Fig. 8 shows the initial and optimized characteristics of the BLC

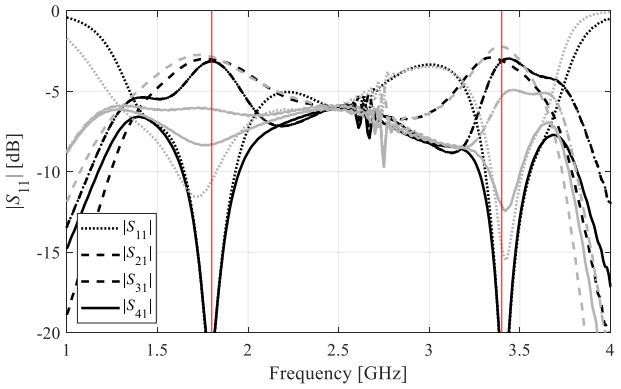

FIGURE 8. Frequency responses of the dual-band BLC of Fig. 6 for the representative run of the multi-resolution algorithm. Target operating frequencies are marked using the vertical lines. The responses at the initial and the final design shown in the top and the bottom panel, respectively.

TABLE 3. Numerical results for branch-line cupler of Fig. 6.

Algorithm	Performance figure							
	Cost[1]	Cost savings[2]	max S_{MI}[3] [dB]	Δmax S_{MI}[4] [dB]	Std S_{MI}[5] [dB]	Max dS[6] [dB]	Δmax dS[7] [dB]	Std dS[8] [dB]
TR search	84.1	-	–14.0	-	2.2	0.1	-	0.15
This work	42.2	50 %	–13.3	0.7	3.6	0.3	0.2	0.48

[1] Number of equivalent high-fidelity EM simulations (averaged over ten algorithm runs).
[2] Relative computational savings in percent w.r.t. the reference algorithm.
[3] $S_{MI} = \max\{S_{11}(\boldsymbol{x},f_1), S_{11}(\boldsymbol{x},f_2), S_{41}(\boldsymbol{x},f_1), S_{41}(\boldsymbol{x},f_2)\}$ (cf. (4)), averaged over ten algorithm runs.
[4] Degradation of S_{MI} w.r.t. the reference algorithm, averaged over ten algorithm runs.
[5] Standard deviation of S_{MI} over the performed algorithm runs.
[6] $dS = [|S_{21}(\boldsymbol{x},f_1) - S_{31}(\boldsymbol{x},f_1)|^2 + |S_{21}(\boldsymbol{x},f_2) - S_{31}(\boldsymbol{x},f_2)|^2]^{1/2}$ (cf. (4)), averaged over ten algorithm runs.
[7] Degradation of dS w.r.t. the reference algorithm, averaged over ten algorithm runs.
[8] Standard deviation of dS over the performed algorithm runs.

obtained for the selected run of the multi-resolution procedure. It can be observed that the multi-resolution approach allows for 50-percent computational savings with respect to the reference algorithm, i.e., the optimization process accelerated by a factor of two. There is a slight degradation of the quality; however, it is not significant. In terms of matching and isolation, it is only 0.7 dB on the average, whereas for the power split error it is 0.2 dB (i.e., worsening from 0.1 dB for the reference algorithm to 0.3 dB for the multi-resolution procedure).

IV. CONCLUSION

In this work, a procedure for expedited design optimization of microwave structures has been proposed. The presented approach employed variable-resolution EM simulations along with the convergence-based management scheme that adjusts the model fidelity depending on the current stage of the optimization process. The major

prerequisites are to utilize the lowest possible resolution at the early stages of the algorithm run to enable computational savings by exploiting the problem-specific knowledge, gradually increase the fidelity in a continuous manner at the middle stages, and conclude the procedure at the high-fidelity level to avoid reliability degradation. By means of comprehensive numerical validation involving two microstrip components, a dual-band power divider, and a dual-band branch-line coupler, our methodology has been demonstrated to permit considerable improvement of computational efficiency as compared to single-fidelity optimization. The savings are as high as almost seventy percent for the power divider, and fifty percent for the BLC. The particular figures are correlated with the simulation time versus model resolution profiles, which are more advantageous for the divider. At the same time, no noticeable quality degradation has been observed in relation to the benchmark.

The knowledge-based optimization approach presented in this paper is a viable alternative to conventional design closure methods. It can be considered a step towards a practical implementation of automated handling of variable-fidelity simulation models within the numerical optimization frameworks. The future work will include the development of further improvements oriented towards achieving additional algorithmic acceleration. The focus will be on incorporating sparse sensitivity updating schemes as well as adaptive tuning of the control parameters of the framework.

ACKNOWLEDGMENT

The authors would like to thank Dassault Systemes, France, for making CST Microwave Studio available.

REFERENCES

[1] Y. Karisan, C. Caglayan, G. C. Trichopoulos, and K. Sertel, "Lumped-element equivalent-circuit modeling of millimeter-wave HEMT parasitics through full-wave electromagnetic analysis," *IEEE Trans. Microw. Theory Techn.*, vol. 64, no. 5, pp. 1419–1430, May 2016.

[2] M. Abdolrazzaghi and M. Daneshmand, "A phase-noise reduced microwave oscillator sensor with enhanced limit of detection using active filter," *IEEE Microw. Wireless Compon. Lett.*, vol. 28, no. 9, pp. 837–839, Sep. 2018.

[3] K.-Y. Tsai, H.-S. Yang, J.-H. Chen, and Y.-J. E. Chen, "A miniaturized 3 dB branch-line hybrid coupler with harmonics suppression," *IEEE Microw. Wireless Compon. Lett.*, vol. 21, no. 10, pp. 537–539, Oct. 2011.

[4] S. Koziel and A. Pietrenko-Dabrowska, "Recent advances in accelerated multi-objective design of high-frequency structures using knowledge-based constrained modeling approach," *Knowl.-Based Syst.*, vol. 214, Feb. 2021, Art. no. 106726.

[5] R. K. Barik, R. Rajender, and S. S. Karthikeyan, "A miniaturized wideband three-section branch-line hybrid with harmonic suppression using coupled line and open-ended stubs," *IEEE Microw. Wireless Compon. Lett.*, vol. 27, no. 12, pp. 1059–1061, Dec. 2017.

[6] J. C. Rautio and S. Arvas, "Measurement of planar substrate uniaxial anisotropy," *IEEE Trans. Microw. Theory Techn.*, vol. 57, no. 10, pp. 2456–2463, Oct. 2009.

[7] P. Li, W. Xu, and D. Yang, "An inversion design method for the radome thickness based on interval arithmetic," *IEEE Antennas Wireless Propag. Lett.*, vol. 17, no. 4, pp. 658–661, Apr. 28, 2018.

[8] S. Chen, D. Ding, M. Yu, Y. Wang, and R. Chen, "Electro-thermal analysis of microwave limiter based on the time-domain impulse response method combined with physical-model-based semiconductor solver," *IEEE Trans. Microw. Theory Techn.*, vol. 68, no. 7, pp. 2579–2589, Jul. 2020.

[9] G. Sun, D. Ayepah-Mensah, A. Budkevich, G. Liu, and W. Jiang, "Autonomous cell activation for energy saving in cloud-RANs based on dueling deep Q-network," *Knowl.-Based Syst.*, vol. 192, Mar. 2020, Art. no. 105347.

[10] Z. He and C. Liu, "A compact high-efficiency broadband rectifier with a wide dynamic range of input power for energy harvesting," *IEEE Microw. Wireless Compon. Lett.*, vol. 30, no. 4, pp. 433–436, Apr. 2020.

[11] D. D. Dinh and M. J. Lancaster, "Microwave power sensors with integrated filtering function for transfer power standards," *IEEE Microw. Wireless Compon. Lett.*, vol. 30, no. 3, pp. 308–311, Mar. 2020.

[12] B. Gowrish and R. R. Mansour, "A novel bandwidth reconfigurable waveguide filter for aerospace applications," *IEEE Microw. Wireless Compon. Lett.*, vol. 30, no. 6, pp. 577–580, Jun. 2020.

[13] D. Psychogiou and R. Gomez-Garcia, "Compact substrate-integrated bandstop filters using double-resonant coaxial resonators," *IEEE Microw. Wireless Compon. Lett.*, vol. 30, no. 10, pp. 941–944, Oct. 2020.

[14] J. Xu, W. Hong, H. Zhang, and H. Tang, "Compact bandpass filter with multiple coupling paths in limited space for Ku-band application," *IEEE Microw. Wireless Compon. Lett.*, vol. 27, no. 3, pp. 251–253, Mar. 2017.

[15] X. F. Ye, S. Y. Zheng, and Y. M. Pan, "A compact millimeter-wave patch quadrature coupler with a wide range of coupling coefficients," *IEEE Microw. Wireless Compon. Lett.*, vol. 26, no. 3, pp. 165–167, Mar. 2016.

[16] P.-L. Chi, Y.-M. Chen, and T. Yang, "Single-layer dual-band balanced substrate- integrated waveguide filtering power divider for 5G millimeter-wave applications," *IEEE Microw. Wireless Compon. Lett.*, vol. 30, no. 6, pp. 585–588, Jun. 2020.

[17] L. Xia, J.-L. Li, B. A. Twumasi, P. Liu, and S.-S. Gao, "Planar dual-band branch-line coupler with large frequency ratio," *IEEE Access*, vol. 8, pp. 33188–33195, 2020.

[18] M. L. Seddiki, M. Nedil, and F. Ghanem, "A novel wide, dual-and triple-band frequency reconfigurable Butler matrix based on transmission line resonators," *IEEE Access*, vol. 7, pp. 1840–1847, 2019.

[19] K. Song, M. Fan, F. Zhang, Y. Zhu, and Y. Fan, "Compact triple-band power divider integrated bandpass-filtering response using short-circuited SIRs," *IEEE Trans. Compon., Packag., Manuf. Technol.*, vol. 7, no. 7, pp. 1144–1150, Jul. 2017.

[20] A. Ebrahimi, T. Baum, J. Scott, and K. Ghorbani, "Continuously tunable dual-mode bandstop filter," *IEEE Microw. Wireless Compon. Lett.*, vol. 28, no. 5, pp. 419–421, May 2018.

[21] H. Ren, B. Arigong, M. Zhou, J. Ding, and H. Zhang, "A novel design of 4×4 Butler matrix with relatively flexible phase differences," *IEEE Antennas Wireless Propag. Lett.*, vol. 15, pp. 1277–1280, 2016.

[22] V.-M.-R. Gongal-Reddy, S. Zhang, C. Zhang, and Q.-J. Zhang, "Parallel computational approach to gradient based EM optimization of passive microwave circuits," *IEEE Trans. Microw. Theory Techn.*, vol. 64, no. 1, pp. 44–59, Jan. 2016.

[23] H. L. Abdel-Malek, A. K. S. O. Hassan, and M. H. Heaba, "A boundary gradient search technique and its applications in design centering," *IEEE Trans. Comput.-Aided Design Integr. Circuits Syst.*, vol. 18, no. 11, pp. 1654–1660, Nov. 1999.

[24] X. Peng, L. Kong, X. Sun, and H. Lyu, "Design and analysis of optical receiving antenna for LED visible light communication based on Taguchi method," *IEEE Access*, vol. 7, pp. 186364–186377, 2019.

[25] X. Li and K. M. Luk, "The grey wolf optimizer and its applications in electromagnetics," *IEEE Trans. Antennas Propag.*, vol. 68, no. 3, pp. 2186–2197, Mar. 2020.

[26] A. A. Al-Azza, A. A. Al-Jodah, and F. J. Harackiewicz, "Spider monkey optimization: A novel technique for antenna optimization," *IEEE Antennas Wireless Propag. Lett.*, vol. 15, pp. 1016–1019, 2016.

[27] F. Gunes, A. Uluslu, and P. Mahouti, "Pareto optimal characterization of a microwave transistor," *IEEE Access*, vol. 8, pp. 47900–47913, 2020.

[28] E. Yigit and H. Duysak, "Determination of optimal layer sequence and thickness for broadband multilayer absorber design using double-stage artificial bee colony algorithm," *IEEE Trans. Microw. Theory Techn.*, vol. 67, no. 8, pp. 3306–3317, Aug. 2019.

[29] A. K. Prasad, M. Ahadi, and S. Roy, "Multidimensional uncertainty quantification of microwave/RF networks using linear regression and optimal design of experiments," *IEEE Trans. Microw. Theory Techn.*, vol. 64, no. 8, pp. 2433–2446, Aug. 2016.

[30] J. S. Ochoa and A. C. Cangellaris, "Random-space dimensionality reduction for expedient yield estimation of passive microwave structures," *IEEE Trans. Microw. Theory Techn.*, vol. 61, no. 12, pp. 4313–4321, Dec. 2013.

[31] M. A. E. Sabbagh, M. H. Bakr, and J. W. Bandler, "Adjoint higher order sensitivities for fast full-wave optimization of microwave filters," *IEEE Trans. Microw. Theory Techn.*, vol. 54, no. 8, pp. 3339–3351, Aug. 2006.
[32] S. Koziel, F. Mosler, S. Reitzinger, and P. Thoma, "Robust microwave design optimization using adjoint sensitivity and trust regions," *Int. J. RF Microw. Comput. Eng.*, vol. 22, no. 1, pp. 10–19, Jan. 2012.
[33] F. Feng, J. Zhang, W. Zhang, Z. Zhao, J. Jin, and Q.-J. Zhang, "Coarse- and fine-mesh space mapping for EM optimization incorporating mesh deformation," *IEEE Microw. Wireless Compon. Lett.*, vol. 29, no. 8, pp. 510–512, Aug. 2019.
[34] J. Zhang, F. Feng, J. Jin, and Q.-J. Zhang, "Efficient yield estimation of microwave structures using mesh deformation-incorporated space mapping surrogates," *IEEE Microw. Wireless Compon. Lett.*, vol. 30, no. 10, pp. 937–940, Oct. 2020.
[35] A. Pietrenko-Dabrowska and S. Koziel, "Computationally-efficient design optimisation of antennas by accelerated gradient search with sensitivity and design change monitoring," *IET Microw., Antennas Propag.*, vol. 14, no. 2, pp. 165–170, Feb. 2020.
[36] S. Koziel and A. Pietrenko-Dabrowska, "Variable-fidelity simulation models and sparse gradient updates for cost-efficient optimization of compact antenna input characteristics," *Sensors*, vol. 19, no. 8, p. 1806, Apr. 2019.
[37] Z. Zhang, Q. S. Cheng, H. Chen, and F. Jiang, "An efficient hybrid sampling method for neural network-based microwave component modeling and optimization," *IEEE Microw. Wireless Compon. Lett.*, vol. 30, no. 7, pp. 625–628, Jul. 2020.
[38] E. Van Nechel, F. Ferranti, Y. Rolain, and J. Lataire, "Model-driven design of microwave filters based on scalable circuit models," *IEEE Trans. Microw. Theory Techn.*, vol. 66, no. 10, pp. 4390–4396, Oct. 2018.
[39] J. L. Chávez-Hurtado and J. E. Rayas-Sánchez, "Polynomial-based surrogate modeling of RF and microwave circuits in frequency domain exploiting the multinomial theorem," *IEEE Trans. Microw. Theory Techn.*, vol. 64, no. 12, pp. 4371–4381, Dec. 2016.
[40] J. E. Rayas-Sánchez, "Power in simplicity with ASM: Tracing the aggressive space mapping algorithm over two decades of development and engineering applications," *IEEE Microw. Mag.*, vol. 17, no. 4, pp. 64–76, Apr. 2016.
[41] D. Gorissen, K. Crombecq, I. Couckuyt, T. Dhaene, and P. Demeester, "A surrogate modeling and adaptive sampling toolbox for computer based design," *J. Mach. Learn. Res.*, vol. 11, pp. 2051–2055, Jul. 2010.
[42] S. Marelli and B. Sudret, "UQLab: A framework for uncertainty quantification in MATLAB," in *Proc. 2nd Int. Conf. Vulnerability Risk Anal. Manage.*, London, U.K., Jul. 2014, pp. 2554–2563.
[43] C. Fu, P. Wang, L. Zhao, and X. Wang, "A distance correlation-based kriging modeling method for high-dimensional problems," *Knowl.-Based Syst.*, vol. 206, Oct. 2020, Art. no. 106356.
[44] Q. Zhou, Y. Wang, P. Jiang, X. Shao, S.-K. Choi, J. Hu, L. Cao, and X. Meng, "An active learning radial basis function modeling method based on self-organization maps for simulation-based design problems," *Knowl.-Based Syst.*, vol. 131, pp. 10–27, Sep. 2017.
[45] F. Feng, W. Na, W. Liu, S. Yan, L. Zhu, J. Ma, and Q.-J. Zhang, "Multifeature-assisted neuro-transfer function surrogate-based EM optimization exploiting trust-region algorithms for microwave filter design," *IEEE Trans. Microw. Theory Techn.*, vol. 68, no. 2, pp. 531–542, Feb. 2020.
[46] J. Cai, J. King, C. Yu, J. Liu, and L. Sun, "Support vector regression-based behavioral modeling technique for RF power transistors," *IEEE Microw. Compon. Lett.*, vol. 28, no. 5, pp. 428–430, May 2018.
[47] A. Petrocchi, A. Kaintura, G. Avolio, D. Spina, T. Dhaene, A. Raffo, and D. M. M.-P. Schreurs, "Measurement uncertainty propagation in transistor model parameters via polynomial chaos expansion," *IEEE Microw. Wireless Compon. Lett.*, vol. 27, no. 6, pp. 572–574, Jun. 2017.
[48] H. M. Torun and M. Swaminathan, "High-dimensional global optimization method for high-frequency electronic design," *IEEE Trans. Microw. Theory Techn.*, vol. 67, no. 6, pp. 2128–2142, Jun. 2019.
[49] L.-Y. Xiao, W. Shao, X. Ding, and B.-Z. Wang, "Dynamic adjustment kernel extreme learning machine for microwave component design," *IEEE Trans. Microw. Theory Techn.*, vol. 66, no. 10, pp. 4452–4461, Oct. 2018.
[50] B. Liu, M. O. Akinsolu, N. Ali, and R. Abd-Alhameed, "Efficient global optimisation of microwave antennas based on a parallel surrogate model-assisted evolutionary algorithm," *IET Microw., Antennas Propag.*, vol. 13, no. 2, pp. 149–155, Feb. 2019.
[51] A. Aldhafeeri and Y. Rahmat-Samii, "Brain storm optimization for electromagnetic applications: Continuous and discrete," *IEEE Trans. Antennas Propag.*, vol. 67, no. 4, pp. 2710–2722, Apr. 2019.
[52] A. Toktas, D. Ustun, and M. Tekbas, "Multi-objective design of multi-layer radar absorber using surrogate-based optimization," *IEEE Trans. Microw. Theory Techn.*, vol. 67, no. 8, pp. 3318–3329, Aug. 2019.
[53] D.-K. Lim, K.-P. Yi, S.-Y. Jung, H.-K. Jung, and J.-S. Ro, "Optimal design of an interior permanent magnet synchronous motor by using a new surrogate-assisted multi-objective optimization," *IEEE Trans. Magn.*, vol. 51, no. 11, Nov. 2015, Art. no. 8207504.
[54] N. Taran, D. M. Ionel, and D. G. Dorrell, "Two-level surrogate-assisted differential evolution multi-objective optimization of electric machines using 3-D FEA," *IEEE Trans. Magn.*, vol. 54, no. 11, Nov. 2018, Art. no. 8107605.
[55] J. W. Bandler, Q. S. Cheng, S. A. Dakroury, A. S. Mohamed, M. H. Bakr, K. Madsen, and J. Sondergaard, "Space mapping: The state of the art," *IEEE Trans. Microw. Theory Tech.*, vol. 52, no. 1, pp. 337–361, Jan. 2004.
[56] S. Li, X. Fan, P. D. Laforge, and Q. S. Cheng, "Surrogate model-based space mapping in postfabrication bandpass Filters' tuning," *IEEE Trans. Microw. Theory Techn.*, vol. 68, no. 6, pp. 2172–2182, Jun. 2020.
[57] S. Koziel and S. D. Unnsteinsson, "Expedited design closure of antennas by means of trust-region-based adaptive response scaling," *IEEE Antennas Wireless Propag. Lett.*, vol. 17, no. 6, pp. 1099–1103, Jun. 7, 2018.
[58] S. Koziel, "Shape-preserving response prediction for microwave design optimization," *IEEE Trans. Microw. Theory Techn.*, vol. 58, no. 11, pp. 2829–2837, Nov. 2010.
[59] C. Zhang, F. Feng, V.-M.-R. Gongal-Reddy, Q. J. Zhang, and J. W. Bandler, "Cognition-driven formulation of space mapping for equal-ripple optimization of microwave filters," *IEEE Trans. Microw. Theory Techn.*, vol. 63, no. 7, pp. 2154–2165, Jul. 2015.
[60] S. Koziel, "Fast simulation-driven antenna design using response-feature surrogates," *Int. J. RF Microw. Comput.-Aided Eng.*, vol. 25, no. 5, pp. 394–402, Jun. 2015.
[61] C.-Y. Cui, Y.-C. Jiao, and L. Zhang, "Synthesis of some low sidelobe linear arrays using hybrid differential evolution algorithm integrated with convex programming," *IEEE Antennas Wireless Propag. Lett.*, vol. 16, pp. 2444–2448, 2017.
[62] M. Pazokian, N. Komjani, and M. Karimipour, "Broadband RCS reduction of microstrip antenna using coding frequency selective surface," *IEEE Antennas Wireless Propag. Lett.*, vol. 17, no. 8, pp. 1382–1385, Aug. 12, 2018.
[63] X. Han, H. Xu, Y. Chang, M. Lin, Z. Wenyuan, X. Wu, and X. Wei, "Multiple diffuse coding metasurface of independent polarization for RCS reduction," *IEEE Access*, vol. 8, pp. 162313–162321, 2020.
[64] S. Koziel and A. Bekasiewicz, "Rapid simulation-driven multiobjective design optimization of decomposable compact microwave passives," *IEEE Trans. Microw. Theory Techn.*, vol. 64, no. 8, pp. 2454–2461, Aug. 2016.
[65] S. Koziel, "Improved trust-region gradient-search algorithm for accelerated optimization of wideband antenna input characteristics," *Int. J. RF Microw. Comput.-Aided Eng.*, vol. 29, no. 4, Apr. 2019, Art. no. e21576.
[66] A. Pietrenko-Dabrowska and S. Koziel, "Expedited antenna optimization with numerical derivatives and gradient change tracking," *Eng. Comput.*, vol. 37, no. 4, pp. 1179–1193, Nov. 2019.
[67] A. Pietrenko-Dabrowska and S. Koziel, "Numerically efficient algorithm for compact microwave device optimization with flexible sensitivity updating scheme," *Int. J. RF Microw. Comput.-Aided Eng.*, vol. 29, no. 7, Jul. 2019, Art. no. e21714.
[68] S. Koziel and S. Ogurtsov, "Model management for cost-efficient surrogate-based optimisation of antennas using variable-fidelity electromagnetic simulations," *IET Microw., Antennas Propag.*, vol. 6, no. 15, pp. 1643–1650, Dec. 2012.
[69] S. Koziel and J. W. Bandler, "Space-mapping optimization with adaptive surrogate model," *IEEE Trans. Microw. Theory Techn.*, vol. 55, no. 3, pp. 541–547, Mar. 2007.
[70] S. Koziel, "Computationally efficient multi-fidelity multi-grid design optimization of microwave structures," *Appl. Comput. Electromagn. Soc. J.*, vol. 25, no. 7, pp. 578–586, 2010.
[71] L. Leifsson and S. Koziel, *Simulation-Driven Aerodynamic Design Using Variable-Fidelity Models*. London, U.K.: Imperial College Press, 2015.
[72] S. Koziel, X. S. Yang, and Q. J. Zhang, *Simulation-Driven Design Optimization and Modeling for Microwave Engineering*. London, U.K.: Imperial College Press, 2013.
[73] U. Ullah, S. Koziel, and I. B. Mabrouk, "Rapid redesign and bandwidth/size tradeoffs for compact wideband circular polarization antennas using inverse surrogates and fast EM-based parameter tuning," *IEEE Trans. Antennas Propag.*, vol. 68, no. 1, pp. 81–89, Jan. 2020.

[74] A. R. Conn, N. I. M. Gould, and P. L. Toint, *Trust Region Methods* (MPS-SIAM Series on Optimization). Philadelphia, PA, USA: SIAM, 2000.
[75] S. Koziel, J. W. Bandler, and K. Madsen, "Space mapping with adaptive response correction for microwave design optimization," *IEEE Trans. Microw. Theory Techn.*, vol. 57, no. 2, pp. 478–486, Feb. 2009.
[76] Y. Su, J. Li, Z. Fan, and R. Chen, "Shaping optimization of double reflector antenna based on manifold mapping," in *Proc. Int. Appl. Comp. Electromagn. Soc. Symp. (ACES)*, Suzhou, China, 2017, pp. 1–2.
[77] A. Pietrenko-Dabrowska and S. Koziel, "Surrogate modeling of impedance matching transformers by means of variable-fidelity electromagnetic simulations and nested cokriging," *Int. J. RF Microw. CAE*, vol. 30, no. 8, 2020, Art. no. e22268.
[78] Z. Lin and Q.-X. Chu, "A novel approach to the design of dual-band power divider with variable power dividing ratio based on coupled-lines," *Prog. Electromagn. Res.*, vol. 103, pp. 271–284, 2010.

SLAWOMIR KOZIEL (Senior Member, IEEE) received the M.Sc. and Ph.D. degrees in electronic engineering from Gdańsk University of Technology, Poland, in 1995 and 2000, respectively, and the M.Sc. degrees in theoretical physics and in mathematics and the Ph.D. degree in mathematics from the University of Gdańsk, Poland, in 2000, 2002, and 2003, respectively. He is currently a Professor with the Department of Engineering, Reykjavik University, Iceland. His research interests include CAD and modeling of microwave and antenna structures, simulation-driven design, surrogate-based optimization, space mapping, circuit theory, analog signal processing, evolutionary computation, and numerical analysis.

ANNA PIETRENKO-DABROWSKA (Senior Member, IEEE) received the M.Sc. and Ph.D. degrees in electronic engineering from Gdańsk University of Technology, Poland, in 1998 and 2007, respectively. She is currently an Associate Professor with Gdańsk University of Technology. Her research interests include simulation-driven design, design optimization, control theory, modeling of microwave and antenna structures, and numerical analysis.

PIOTR PLOTKA received the M.Sc. and D.Eng. degrees in electronic engineering from Gdańsk University of Technology, Poland, in 1976 and 1985, respectively, and the D.Sc. degree in electronic engineering from the Institute of Electron Technology, Warsaw, Poland, in 2008. Since 1981, he has been with Gdańsk University of Technology. In 1990, he joined the Nishizawa Terahertz Project of Research Development Corporation of Japan, Sendai, where he was developing device applications of GaAs molecular layer epitaxy. From 1992 to 2008, he worked as a Senior Researcher with the Semiconductor Research Institute, Sendai. He led a group developing nanometer-scale GaAs static induction transistors for application in future communication circuits. Since 2008, he has also been with the Gdańsk University of Technology. His current research interests include fabrication and physics of operation of poly- and nano-crystalline diamond devices and sensors for electrochemical applications.